Article

Redox Cascades and Making of a C-C Bond: 1,2-Benzodiazinyl Radicals and a Copper Complex of a Benzodiazine

Sandip Mondal, Sachinath Bera, and Prasanta Ghosh

Just Accepted

Redox Cascades and Making of a C-C Bond: 1,2-Benzodiazinyl Radicals and a Copper Complex of a Benzodiazine

Sandip Mondal, Sachinath Bera and Prasanta Ghosh[a]

Department of Chemistry, R. K. Mission Residential College, Narendrapur, Kolkata 103, West Bengal,

India

E-mail: ghosh@pghosh.in

1

ABSTRACT

Two 1,2-benzodiazinyl radicals, cinnolinyl radicals by name, were successfully isolated by cascade routes using 1,4-naphthoquinone as a precursor. Reaction of 1,4-naphthoquinone with hydrazine hydrate promotes a $(5e + 5H^+)$ redox cascade affording benzo[g]naphtho[1,2-c]cinnolinyl-7,12,14-trione ($Cn^\bullet$) in 69% yields, while the similar reaction with 2-hydrazinopyridine is a $(7e + 7H^+)$ oxidative cascade and furnishes N-pyridinecinnolinyl radical ($^{Py}Cn^\bullet$). The cascades are composed of C-N and C-C bond making reactions. The neutral even alternate arenes are always diamagnetic, thus the isolation of $Cn^\bullet$ and $^{Py}Cn^\bullet$ is a breakthrough. The $Cn^\bullet/Cn^-$ and $^{Py}Cn^\bullet/^{Py}Cn^-$ redox couples are reversible and the reaction of $Cn^\bullet$ with $[Cu^I(PPh_3)_3Cl]$ in presence of hydrazine hydrate and Et_3N affords a Cn^- complex of copper(I), $[(Cn^-)Cu^I(PPh_3)_2]$ (**1**). Similar to phenalenyl radical, $^{Py}Cn^\bullet$ exists in three redox states, $^{Py}Cn^+$, $^{Py}Cn^\bullet$, $^{Py}Cn^-$ in a smaller potential range (-0.30 V to -0.60 V *vs* Fc^+/Fc couple) and can be used as an oxidant as well as a reductant. $^{Py}Cn^\bullet$ acts as a catalyst for the oxidative cleavages of benzil to benzoic and 2,2'-pyridil to picolinic acids in methanol in presence of air. The molecular and electronic structures of $Cn^\bullet$, $^{Py}Cn^\bullet$ and **1**.½MeOH were confirmed by single crystal X-ray crystallography, EPR spectroscopy and DFT calculations.

2

Introduction

Paramagnetic neutral odd alternate hydrocarbon (OAH) where the unpaired electron resides on a non bonding molecular orbital is a threshold in designing non metal super conductors proposed by Haddon.[1] In this regard phenalenyl, an OAH was explored widely in elucidating super conductivity,[2] catalytic activity,[3] designing memory devices[4] and the results are promising in many cases. The growth of hydrocarbon radical chemistry visited is based on the skeleton constituted of phenalenyl fragment. The neutral even alternate hydrocarbons which are abundant are diamagnetic and lack this important feature. However, the scope remains open for the hetero-arene incorporating NH functions that are oxidizable to N$^•$ as established in case of Blatter radical.[5] In such cases neutral even alternate hetero-arene can be paramagnetic. In this study, the same was established by isolating two neutral even alternate paramagnetic hetero-arenes as 1,2-benzodiazinyl radicals. Benzodiazines are a class of azine compounds that exhibit diverse biological activities.[6] These were worthy in medicinal and agro-chemistry.[7] Several routes were developed in synthesizing benzodiazine derivatives.[8] However, no paramagnetic benzodiazine derivative is reported so far.

In this investigation we succeeded to design redox cascades that furnish hither-to-unknown 1, 2-benzodiazinyl radicals. Cascades that have high atom economy with lower chemical waste are worthy in devoloping the syntheses of functional organic molecules.[9] However, examples of redox cascades are limited in scope.[10] Recently we have disclosed that 1,4-naphthoquinone derivatives are precursors of redox cascades.[11] In this particular search, two stable 1, 2 benzodiazinyl radicals as illustrated in Chart 1, benzo[g]naphtho[1,2-c]cinnolinyl-7,12,14-trione (Cn$^•$) and N-pyridinecinnolinyl (^{Py}Cn$^•$) radicals by name were successfully isolated in high yields exploiting 1,4-naphthoquinone as a precursor. It is noteworthy that Cohen in 1966 claimed that 1, benzo[g]naphtho[1,2-c]cinnoline-7,12,14-trione (CnH) was isolated from a reaction of 1,4-naphthoquinone with hydrazine hydrate in methanol.[12a] Pummerer *et.al.* in 1929 also reported the isolation of CnH from a reaction of 2,2'-dinaphthoqinone with hydrazine hydrate.[12b] Both of them considered that they had isolated the diamagnetic CnH with a para magnetic impurity and missed to assign the Cn$^•$. In this report, it is disclosed that reaction of 1,4-naphthoquinone

3

with hydrazine hydrate in air promotes a redox cascade affording Cn$^\bullet$ as a major product, no CnH was isolated from this reaction. The similar reaction of 1,4-naphthoquinone with 2-hydrazinopyridine yields ^{Py}Cn$^\bullet$. The structural skeletons of Cn$^\bullet$ and ^{Py}Cn$^\bullet$ are different, the former contains an 1,4-iminoquinone fragment. The redox activity of Cn$^\bullet$ is notably different from ^{Py}Cn$^\bullet$ that resembles with the chemistry of phenalenyl. Notably, the properties of Cn$^\bullet$ and ^{Py}Cn$^\bullet$ are different from common hydrazyl radicals.[13]

Chart 1. Isolated 1, 2-Benzodiazinyl Radicals and a Copper Complex

Cn$^\bullet$ ^{Py}Cn$^\bullet$ **1**
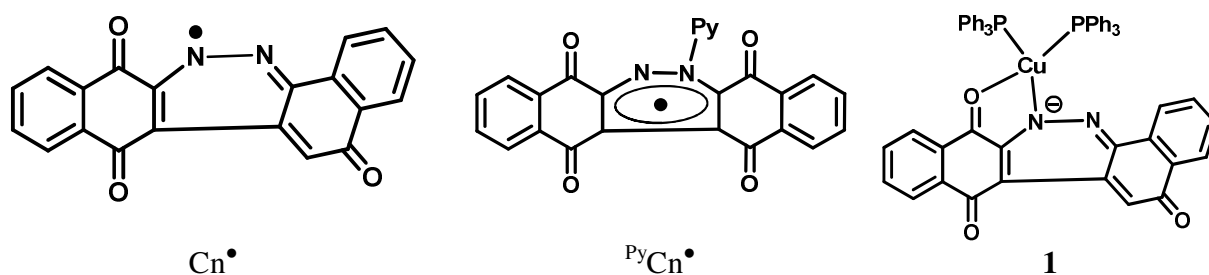
Isolation of a stable cinnolinyl radical that belongs to an even alternate hydrocarbon family is a milestone to the growth of the chemistry of neutral paramagnetic aromatics and designing functional materials and devices. The preliminary investigation establishes that ^{Py}Cn$^\bullet$ acts as a catalyst for the oxidative cleavage of benzil to benzoic acid in methanol in presence of air. Oxidative cleavage of benzil to benzoic acid is not common, generally in presence of base benzil undergoes rearrangement to benzilic acid.[14] Thus, modelling of a catalyst for this redox reaction is significant in metallo-organic chemistry and in this regard, the activity of ^{Py}Cn$^\bullet$ is worthy.

Transition metal complexes of Cn$^\bullet$ will be a venue to stabilize other redox states of it and to open up the possibilities of their inter-conversions detecting the spectral and structural features and the activities. In this context, the first benzodiazinate complex of a transition metal ion is reported. In this particular study, a cinnolinate (Cn$^-$) complex of copper(I), of type [(Cn$^-$)Cu^I(PPh$_3$)$_2$] (**1**) was isolated and characterized. The molecular and electronic structures of Cn$^\bullet$, ^{Py}Cn$^\bullet$ and **1** were confirmed by single crystal X-ray crystallography, EPR spectroscopy, cyclic voltammetry and density functional theory (DFT) calculations.

Results and Discussion

Details of the syntheses of $Cn^{\bullet}$, $^{Py}Cn^{\bullet}$ and **1** and their characterization data are outlined in the Experimental Section (*vide infra*). Reaction of 1,4-naphthoquinone with hydrazine in methanol promotes a redox cascade affording $Cn^{\bullet}$ in 69% yields. The plausible path of the cascade are shown in Scheme 1. The reaction procedes via 1,4 addition reaction of hydrazine to 1,4-naphthoquinone followed by tautomerization affording **A.** In presence of air as an oxidizing agent, **A** undergoes oxidation, tautomerization, oxidation, condensation and further oxidation furnishing $Cn^{\bullet}$. The conversion of **A** to $Cn^{\bullet}$ in air is faster and no intermediate of this transformation has been successfully detected. In the ESI mass spectrometry, the reaction mixture just after 2 min gives a single m/z peak at 325 due to $Cn^{\bullet}$ (Figure S1). In presence of air, the reaction produces H_2O_2 which was detected chemically by recating with KI solution evolving I_2. In presence of starch, the broader Uv-vis absorption band at 600 nm of the reaction mixtute (Figure S2) infers the formation of a starch-I_2 complex.[15a] It is similar to the antharaquinone process of H_2O_2 production.[15b] The study concludes that the conversion of 1,4-naphthoquinone to $Cn^{\bullet}$ in presence of hydrazine is a redox reaction. It is overall a ($5e + 5H^+$) oxidative coupling reaction as given in eq 1.

$$\text{1,4-Naphthoquinone} + NH_2NH_2 + 2O_2 = Cn^{\bullet} + 5/2\ H_2O_2 + H_2O \qquad (1)$$
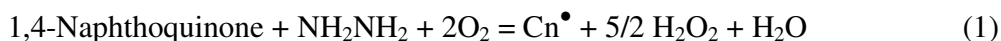
However, in absence of air the reaction is slower and different as depicted in Scheme 1. Analysis of the reaction mixture under argon by ESI mass spectrometry confirmed the formation of **A** and a hydroquinone derivative **B** as given in Figure S3. In presence of I_2 **B** undergoes oxidation to **C** that gives the product $Cn^{\bullet}$, where I_2 is reduced to iodide. Pummerer *et.al.*[12b] established that **C** is a precursor of $Cn^{\bullet}$, supporting the notion of formation of **C** as an intermediate of this oxidative coupling reaction in presence of air and I_2. The formation of iodide was authenticated by detecting mass peaks due to iodide and a monoiodo adduct of $Cn^{\bullet}$ in ESI mass spectrometry (Figure S4). The study infer that the conversion of 1,4-naphthoqione $\rightarrow Cn^{\bullet}$ in presence of hydrazine needs an oxidizing agent.

Scheme 1. Redox Cascade and Formation of **Cn$^\bullet$**
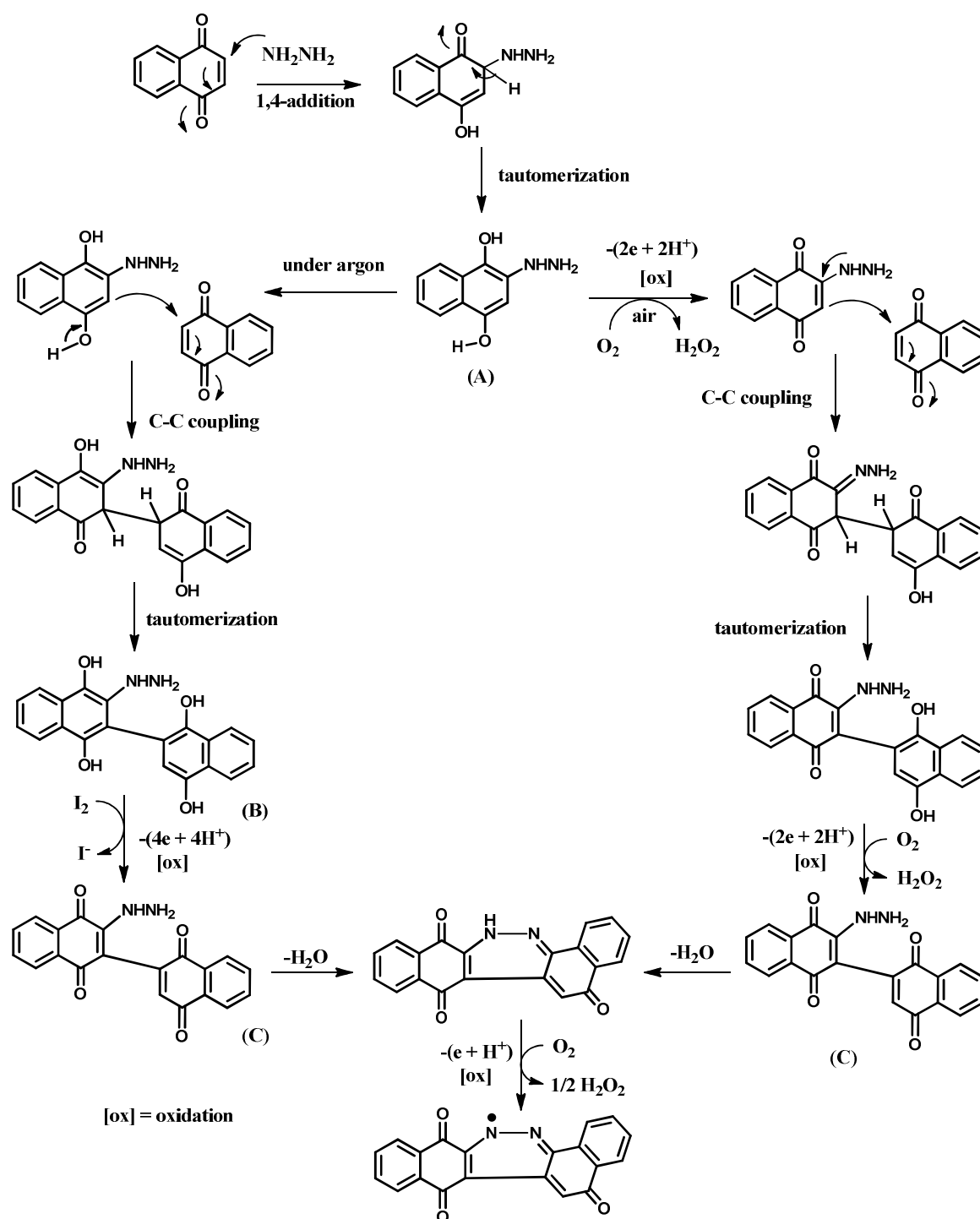
The similar reaction with phenylhydrazine produces naphthalene-1,4-diol evolving nitrogen gas, while the reaction of 1,4-naphthoquinone with less reducing 2-hydrazinopyridine promotes a different cascade affording ^{Py}Cn$^\bullet$ in 71% yields. It is a (7e+7H$^+$) oxidative dimerization of two 1,4-
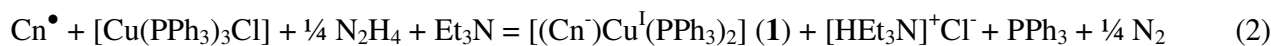
naphthoquinone units bridged by hydrazinopyridine fragment. The cascade is composed of 1,4 addition

reaction (C-N bond formations),

Scheme 2. Redox Cascade and Formation of ^{Py}**Cn**$^\bullet$
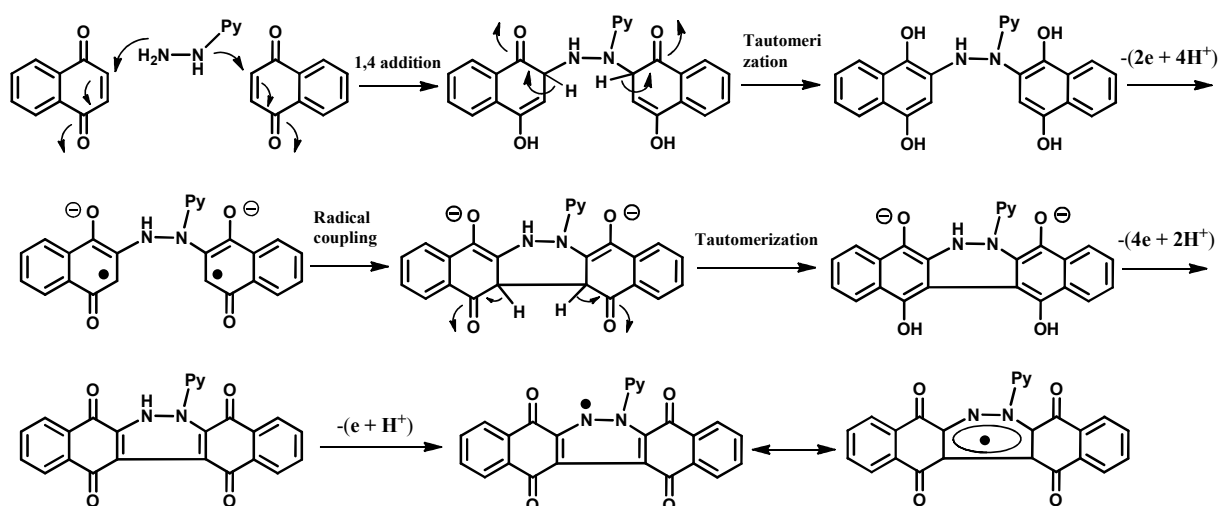
tautomerization, oxidation, radical coupling (C-C bond formation) reactions, and oxidation of amine to

aminyl radical as depicted in Scheme 2. The intermediates of these reactions were analyzed by ESI mass

spectrometry. The concerted 1,4-addition of the hydrazine derivative with two 1,4-naphthoquinones

were authenticated by ESI mass spectrometry of the solution obtained after 5 min of both reactions (see,

Figure S5). Notably no mass peak due to mono hydrazine-1,4-naphthoquinone derivative was detected.

The reaction of Cn$^\bullet$ with [Cu^I(PPh$_3$)$_3$Cl] in presence of Et$_3$N in a mixture of methanol and

dichloromethane solvents does not yield any isolable product, however the same reaction in presence of

hydrazine hydrate at room temperature affords green crystals of **1** in 57% yields. In this reaction,

hydrazine acts as a reductant converting Cn$^\bullet$ to Cn$^-$. The reaction is expressed by eq 2.

$$Cn^\bullet + [Cu(PPh_3)_3Cl] + \tfrac{1}{4} N_2H_4 + Et_3N = [(Cn^-)Cu^I(PPh_3)_2] \, (\mathbf{1}) + [HEt_3N]^+Cl^- + PPh_3 + \tfrac{1}{4} N_2 \qquad (2)$$

X-ray Crystallography. ^{Py}**Cn**$^\bullet$ and **1**.1/2MeOH crystallize respectively in *P*-1 and *P*2$_1$/*C* space

groups (CCDC 1835620 and 1872411). The molecular geometries in the crystal forms and the atom

labeling scheme are illustrated in Figure 1, Figures S6(a) and S6(b). The crystallographic data are

summarized in Table S1. The selected bond parameters are listed in Table 1. In ^{Py}**Cn**$^\bullet$, the N(1)-N(2)

length is 1.367(2) Å that corresponds well to that of the zwitterionic triphenylphosphonio-hydrazyl

7

radical reported recently.[11] The N(1)-C(2) length, 1.291(2) Å is relatively shorter due to the conjugation of the singly occupied p orbital of the N(1) atom with the benzoquinone fragment. For the same reason the C(2)-C(3) and C(4)-O(2) lengths are relatively longer than C(11)-C(12) and C(1)-O(1) lengths. The N(2)-C(11) is 1.371(2) Å. The non-bonded distance between two successive layers in $^{Py}Cn^{\bullet}$ is 3.360 Å, implying that no significant interaction between two paramagnetic units is present in crystals and the same was authenticated by EPR spectroscopy.

For comparison, the bond parameters of $^{Py}Cn^{\bullet}$ in gas phase were elucidated by hybrid B3LYP DFT method. The gas phase geometry of $^{Py}Cn^{\bullet}$ was optimized with doublet spin state using 6-31+G(d,p) basis set and calculated bond parameters are listed in Table 1. The calculated lengths except C(3)-C(4) length, correlate well with those obtained from single crystal diffraction study. Notably, both calculated and experimental N-N lengths of $^{Py}Cn^{\bullet}$ are relatively longer than N=N length due to localization of the unpaid electron. The N-N length in azo anion radicals lies in the range of 1.33-1.34 Å.[16]

We failed to isolate the single crystals for X-ray diffraction study of $Cn^{\bullet}$. However, a Cn^{-} complex of copper(I) as in **1**.½MeOH has been structurally characterized. The X-ray bond parameters of $^{Py}Cn^{\bullet}$ and Cn^{-} in **1**.½MeOH are notably different. The CuP_2NO tetrahedron of **1**.½MeOH is distorted. In **1**.½MeOH the N(1)-N(2) length, 1.341(3) Å, is relatively shorter than that in $^{Py}Cn^{\bullet}$. The N(1)-C(2) length is an intermediate between C-N single and double bonds. The C(3)-C(12) length is also shorter than a $C_{sp2}-C_{sp2}$ length. The features can be analyzed by the resonance structures of Cn^{-} as given in Chart 2, where the **E** and **F** forms are aromatic in nature. Due to the resonance contribution, the C(14)-O(3) length is relatively longer than C(1)-O(1) and C(4)-O(2) lengths. The 1,4-naphthoquinone is a weaker ligand and the Cu-O(1) length, 2.247(2) Å is significantly longer than the Cu-N(1) length, 2.012(2) Å. Because of the coordinated anionic ligand, the Cu(I) → PPh3 back-bonding is stronger and the average Cu-PPh3 lengths, 2.238 (1) Å, are relatively shorter than those recorded in bis(triphenylphosphine) complexes of copper(I) containing neutral polypyridyl ligands. For example, in [Cu(PPh3)2dppz]NO3 (dppz = dipyridophenazine), the average Cu-PPh3 lengths are 2.271(1) Å.[17]

Chart 2. Resonance Structures of Cn⁻

D   E   F

(a)   (b)
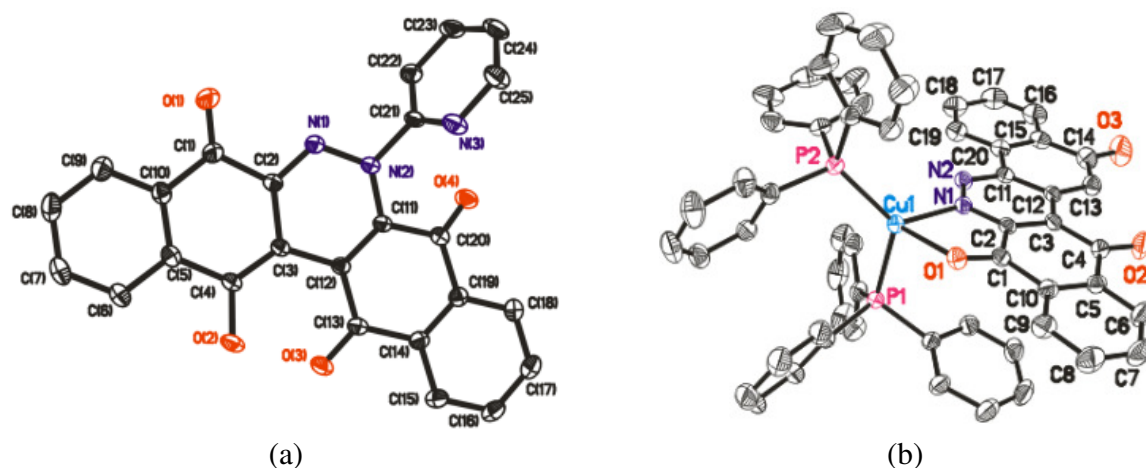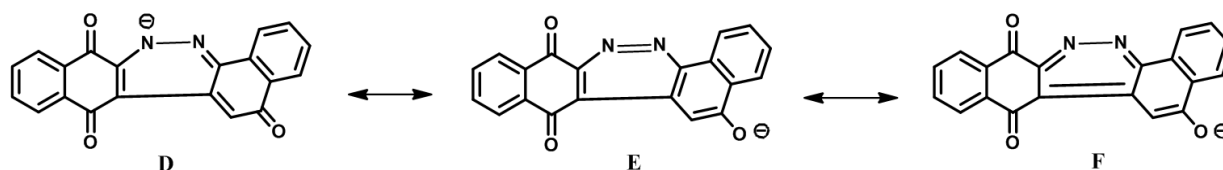
Figure 1. Molecular geometries of (a) $^{Py}Cn^\bullet$ and (b) **1**.½MeOH in crystal forms (40% thermal ellipsoids, hydrogen atoms and solvent molecule are omitted for clarity).

Table 1. Selected Experimental and Calculated Bond Lengths of (Å) of $^{Py}Cn^\bullet$

	Exptl	Calcd		Exptl	Calcd
N(1)-N(2)	1.367(2)	1.359	C(3)-C(12)	1.487(2)	1.430
N(1)-C(2)	1.291(2)	1.313	O(3)-C(13)	1.238(2)	1.220
C(2)-C(3)	1.465(2)	1.427	O(4)-C(20)	1.212(2)	1.223
C(3)-C(4)	1.367(2)	1.465	N(2)-C(11)	1.371(2)	1.390
C(1)-O(1)	1.212 (2)	1.221	C(11)-C(12)	1.368(2)	1.380
C(4)-O(2)	1.346(2)	1.301	C(12)-C(13)	1.473(2)	1.501

The bond parameters of **1**, **1⁺**, Cn⁺ and CnH were calculated by hybrid PBE0 DFT method to establish the trend of bond lengths of different redox forms. The gas phase geometries of **1** and CnH were optimized with singlet spin state, while those of **1⁺** and Cn⁺ were optimized with doublet spin state. The calculated bond lengths are summarized in Table 2. The calculated N-N lengths of **1** and CnH are similar. In the conversion of **1** → **1⁺**, no significant changes of Cu-N(1), Cu-O(1) and Cu-P lengths were

observed. Notably, the calculated N-N lengths of 1^+ and $Cn^\bullet$ are comparable, inferring that 1^+ is a

copper(I) complex of $Cn^\bullet$.

Table 2. Selected Experimental Bond Lengths of (Å) of **1**.½MeOH and Calculated Bond Lengths of (Å)

1, 1^+, $Cn^\bullet$ and CnH

	Exptl		Calcd		
1.½MeOH		**1**	1^+	$Cn^\bullet$	CnH
Cu-N(1)	2.012 (2)	2.046	2.025		
Cu-O(1)	2.247(2)	2.254	2.246		
Cu-P(1)	2.262(2)	2.324	2.324		
Cu-P(2)	2.214(2)	2.272	2.297		
N(1)-N(2)	1.341(3)	1.326	1.314	1.309	1.329
N(1)-C(2)	1.344(3)	1.399	1.348	1.344	1.344
C(2)-C(3)	1.396(3)	1.398	1.393	1.401	1.382
C(3)-C(4)	1.473(4)	1.463	1.498	1.504	1.485
C(1)-O(1)	1.230(5)	1.232	1.227	1.217	1.222
C(4)-O(2)	1.222(3)	1.223	1.213	1.222	1.225
C(3)-C(12)	1.437(3)	1.449	1.426	1.429	1.458
N(2)-C(11)	1.327(3)	1.327	1.315	1.340	1.308
C(11)-C(12)	1.443(4)	1.462	1.447	1.439	1.475
C(12)-C(13)	1.390(4)	1.377	1.400	1.412	1.375
C(13)-C(14)	1.414(4)	1.445	1.456	1.455	1.450
C(14)-O(3)	1.256(4)	1.228	1.224	1.238	1.237

Redox Activity. The redox activities of $Cn^\bullet$, **1** and $^{Py}Cn^\bullet$ were investigated by cyclic voltammetry in

acetonitrile at RT using tetrabutylammonium hexafluorophosphate as a supporting electrolyte and the

potential data referenced to Fc^+/Fc couple are listed in Figure 2. The cyclic voltammogram of $Cn^\bullet$

displays two cathodic waves respectively at -1.14 and -1.56 V (Figure 2(a)) due to $Cn^\bullet/Cn^-$ and Cn^-

$/Cn^{\bullet 2-}$ redox couples (Scheme 3).
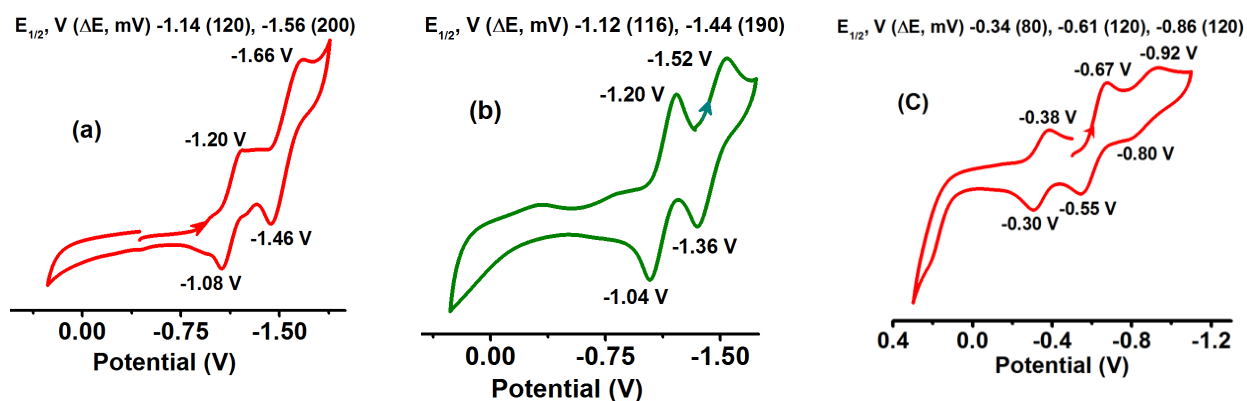
Figure 2. Cyclic voltammograms of (a) Cn$^\bullet$, (b) **1** and (c) ^{Py}Cn$^\bullet$ in acetonitrile using tetrabutylammonium hexafluorophosphate as a supporting electrolyte (Potential referenced to Fc$^+$/Fc couple).

The cyclic voltammogram of **1** is exactly similar to that of Cn$^\bullet$ (Figure 2(b)), precluding the mixing of the metal with benzodiazine ligand. The anodic Cn$^\bullet$/Cn$^-$ redox couple of **1** appears at -1.12 V, while the same for free Cn$^\bullet$ is observed at -1.14 V. The cathodic Cn$^-$/Cn^{2-} redox wave of **1** appears at -1.44 V.

The redox activity of ^{Py}Cn$^\bullet$ is different from Cn$^\bullet$ and **1** (Figure 2(c)). Notably, the cyclic voltammogram of ^{Py}Cn$^\bullet$ is similar to that of phenalenyl. ^{Py}Cn$^\bullet$ exhibits a reversible anodic wave at - 0.34 V due to ^{Py}Cn$^+$/^{Py}Cn$^\bullet$ redox couple. The first cathodic wave at - 0.61 V due to ^{Py}Cn$^\bullet$/^{Py}Cn$^-$ is quite reversible, while the second cathodic wave at -0.86 V due to 1,4-naphthoquinone/1,4-naphthosemiquinonate anion radical redox couple is not reversible. In comparison to Cn$^\bullet$/Cn$^-$ redox couple, the ^{Py}Cn$^\bullet$/^{Py}Cn$^-$ couple is positively shifted by 0.53 V, inferring that ^{Py}Cn$^\bullet$ is stronger reducing than Cn$^\bullet$. Similarly the second cathodic wave due to quinone reduction is positively shifted by 0.70 V. The study infers that ^{Py}Cn$^\bullet$ is an oxidizing as well as a reducing agent. It exists in three redox states as ^{Py}Cn$^+$, ^{Py}Cn$^\bullet$ and ^{Py}Cn$^-$ as depicted in Scheme 3, in a smaller potential range (-0.30 to -0.60 V) and ^{Py}Cn$^\bullet$ is a stable state and isolable in air.

Scheme 3. Redox Series of Cn$^\bullet$ and ^{Py}Cn$^\bullet$
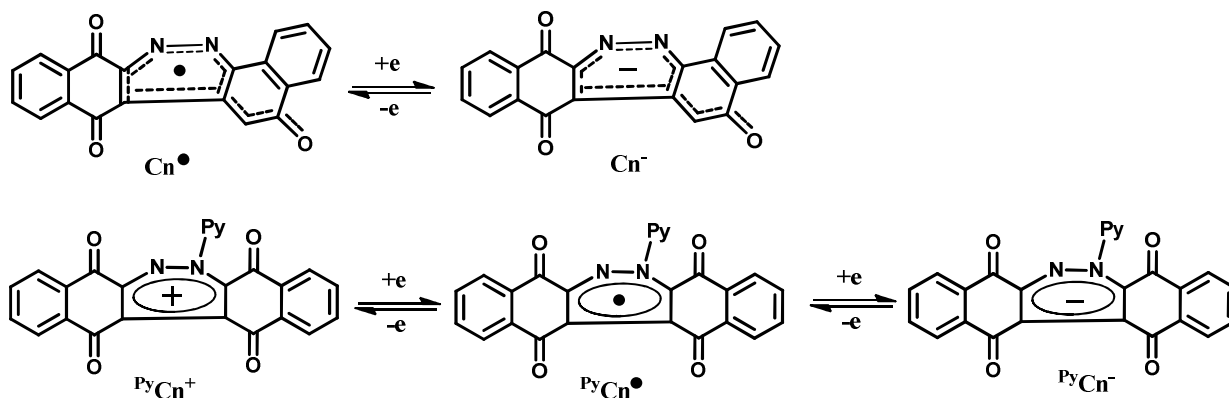
EPR Spectroscopy and DFT Calculations. The X-band EPR spectrum of the powder sample of Cn$^\bullet$

exhibits a strong signal at g = 2.002 as illustrated in Figure 7(a), correlating well with those of organic

radicals.[18] The isotopic signal of Cn$^\bullet$ in CH_2Cl_2 at g = 2.003 (Figure S7(b)) does not reveal any

hyperfine splitting. The fluid solution EPR spectrum of $\mathbf{1}^+$ obtained from a constant potential (at -0.80

V) bulk electrolysis experiment in CH_2Cl_2 displays a strong EPR
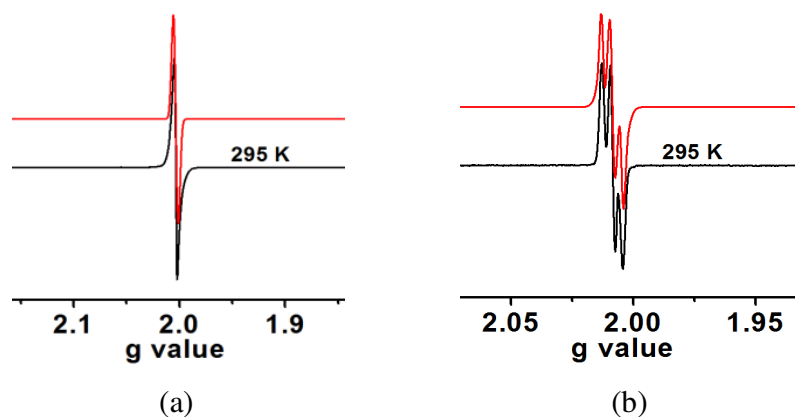
Figure 3. X-band EPR spectra of ^{Py}Cn$^\bullet$ (a) powder Sample at 295 K (b) CH_2Cl_2 solution at 295 K.

(Experimental, black and simulated, red).

signal at g = 2.0014 (Figure S7(c)), authenticating that $\mathbf{1}^+$ is a Cn$^\bullet$ complex of copper(1). The powder

sample spectrum of ^{Py}Cn$^\bullet$ displays a strong signal at g = 2.003 (Figure 3(a)). The fluid solution

spectrum of ^{Py}Cn$^\bullet$ shows a hyperfine splitting due to ^{14}N nucleus (I = 1, A$_N$ = 6.4 G) as depicted in

Figure 3(b). However, the frozen glass spectrum of ^{Py}Cn$^\bullet$ with a signal at g = 2.003 does not display any

hyperfine splitting.

The spin density distributions of Cn$^\bullet$ and ^{Py}Cn$^\bullet$ obtained from Mulliken spin population analyses are illustrated in Figures 4(a) and 4(b). In both cases the spin is dominantly localized on the benzodiazine ring. In Cn$^\bullet$, the alpha spin scatters on N(1) (18%), C(3) (27%) and C(11) (15%) atoms, while the beta spin disperses on the alternate C(2), C(12) and N(2) atoms. In addition the alpha spin is significantly localized on C(3) (61%) and O(3) (26%) atoms. In case of ^{Py}Cn$^\bullet$, the maximum alpha spin bearing atom is C(3) carbon (41%) and the rest is localized on N(1), N(2), C(11) and O(2) atoms, while the beta spin is localized on C(2) and C(12) atoms. It implies that the benzodiazine ring actively participate in both oxidation and reduction reactions. Formation of a C-C sigma bond enhances the quenching of the phenalenyl radical, however in case of ^{Py}Cn$^\bullet$ no dimerization occurs as the C(3) atom is a member of two fused rings. Two significant frontier molecular orbitals of ^{Py}Cn$^\bullet$, SOMO and beta-LUMO of this unique hetero-arene dominantly disperse on the benzodiazine ring, while the alpha-LUMO scatters on one of the 1,4-naphthoquinone fragments as depicted in Figure S8.

        (a)   (b)   (c)
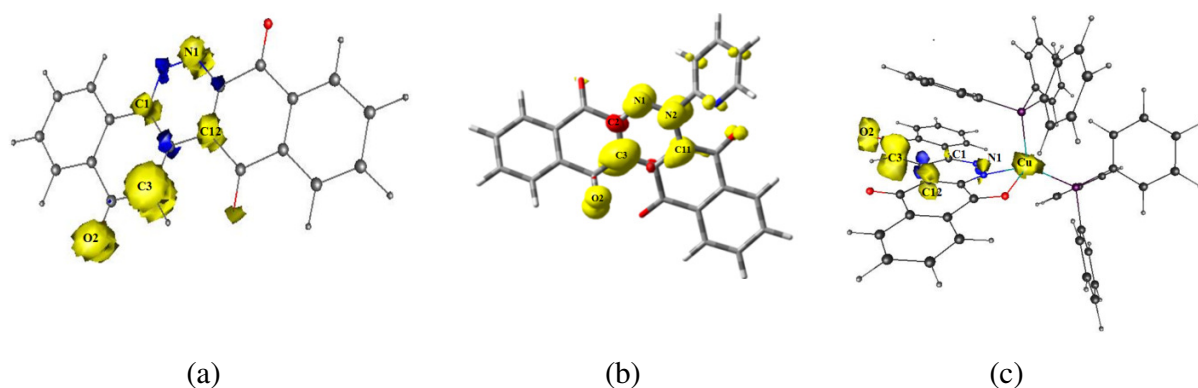
Figure 4. Spin density plots of (a) Cn$^\bullet$ (N1, 0.18; N2, -0.08; C2, -0.11; C3, 0.23; C11, 0.17; C12, -0.20; C13, 0.61; O3, 0.26), (b) ^{Py}Cn$^\bullet$ (N1, 0.23; N2, 0.16; C3, 0.41; C11, 0.12; O2, 0.15) and (c) **1**$^+$ (N1, 0.15; N2, -0.08; C2, -0.13; C3, 0.27; C11, 0.15; C12, -0.20; C13, 0.59; O3, 0.25) obtained from Mulliken spin population analyses.

    It is noteworthy that the calculated electron affinity of ^{Py}Cn$^\bullet$ is relatively larger (2.69 eV), while the calculated ionization energy is smaller (6.50 eV) and comparable to those of alkaline earth metals. The calculated energies of the frontier molecular orbitals of ^{Py}Cn$^+$, ^{Py}Cn$^\bullet$ and ^{Py}Cn$^-$ are depicted in Figure 5. The HOMO of ^{Py}Cn$^+$ is stabilized by 8.74 eV than that of ^{Py}Cn$^-$. Similarly, the LUMO of ^{Py}Cn$^+$ is 7.43

eV lower in energy than that of $^{Py}Cn^-$. The energy of SOMO of $^{Py}Cn^\bullet$ is an intermediate between that of the HOMOs of $^{Py}Cn^+$ and $^{Py}Cn^-$. The analysis predicts that $^{Py}Cn^\bullet$ is a stronger reducing agent and the same was established by cyclic voltammetry and chemical activities.
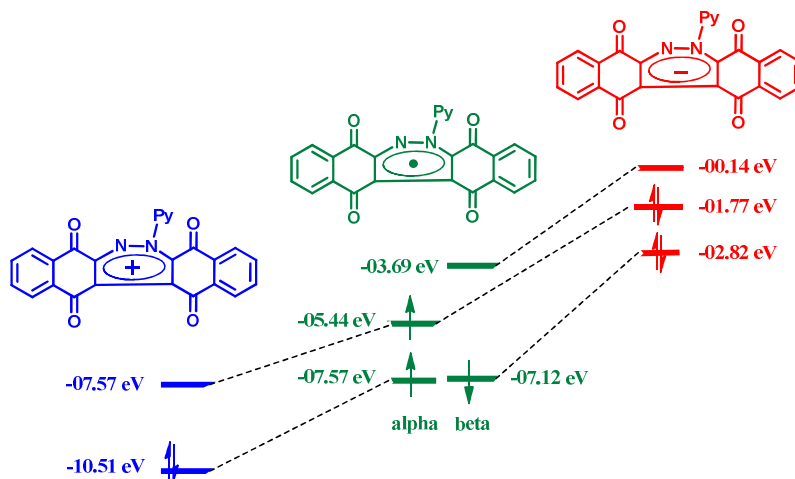
Figure 5. Relative calculated energies of the frontier molecular orbitals of $^{Py}Cn^+$, $^{Py}Cn^\bullet$ and $^{Py}Cn^-$.

The calculated bond lengths of **1** and CnH are summarized in Table 2. The calculated bond lengths of Cn$^-$ in **1** correlates well with those of CnH, particularly the N(1)-N(2) lengths are 1.326 and 1.329 Å respectively in **1** and CnH. However, the bond lengths of the benzodiazine ring in **1**$^+$ are similar to those of Cn$^\bullet$. The N(1)-N(2) lengths of **1**$^+$ and Cn$^\bullet$ are 1.314 and 1.309 Å respectively. The spin density distribution of **1**$^+$ ion as depicted in Figure 4(c) is also similar to that of Cn$^\bullet$ confirming that **1**$^+$ is a Cn$^\bullet$ complex of copper(I).

Electronic Spectra. The UV-vis-NIR absorption spectra of Cn$^\bullet$, **1** and $^{Py}Cn^\bullet$ were recorded in CH_2Cl_2 and the spectra are shown in Figures 6(a) and 6(b). The spectrum of Cn$^\bullet$ displays an absorption band at 530 nm. The absorption spectra of Cn$^\bullet$ and Cn$^-$ forms are different. **1** containing Cn$^-$ as a ligand exhibits a lower energy broader band at 720 nm and the characteristic bands at 470 and 450 nm. The absorption feature of free Cn$^-$ ion was recorded by spectro-electrochemical measurement (Figure 7 (a)). Cn$^-$ reveals absorption bands at 750, 500 and 480 nm.
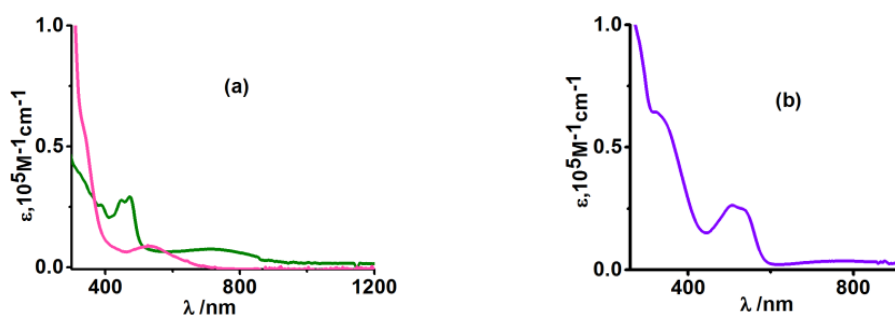
Figure 6. UV-vis-NIR absorption spectra of (a) Cn$^\bullet$ (red) and **1** (green) and (b) ^{Py}Cn$^\bullet$ in CH$_2$Cl$_2$.
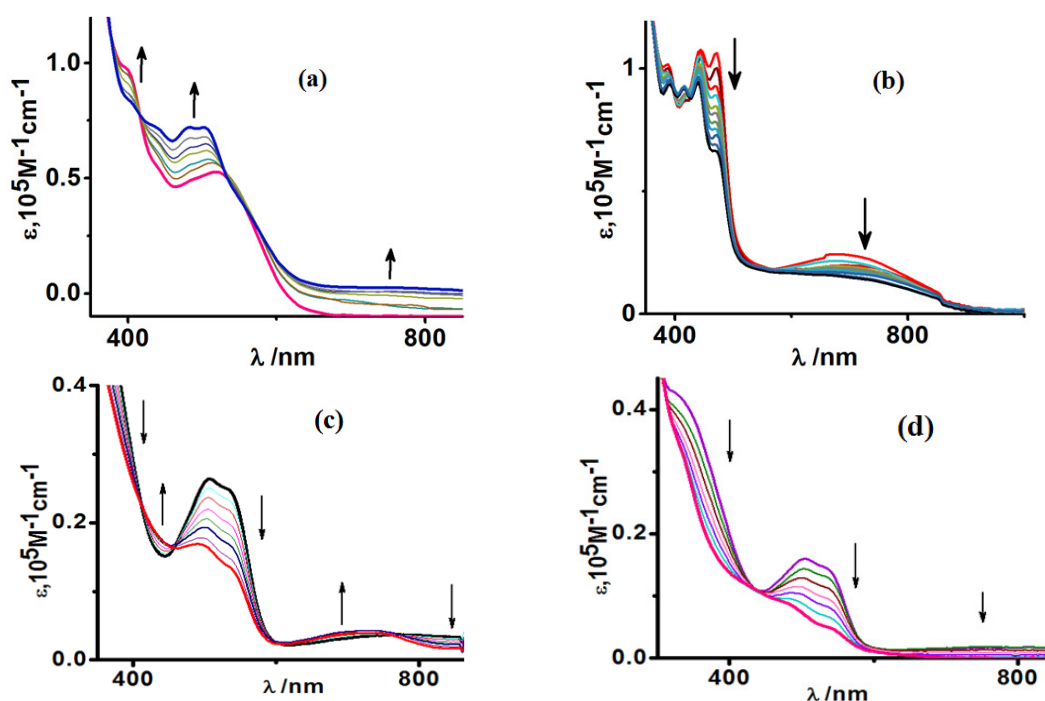
Figure 7. Spectral changes during (a) Cn$^\bullet \to$ Cn$^-$, (b) **1**$\to$ **1**$^+$, (c) ^{Py}Cn$^\bullet \to$ ^{Py}Cn$^+$ and (d) ^{Py}Cn$^\bullet \to$ ^{Py}Cn$^-$

conversions recorded by spectroelectrochemical measurements in CH$_2$Cl$_2$ at 295 K.

The feature is similar to that of **1**, only bands are red shifted by 30 nm. Thus the lower energy

absorption band of **1** at 720 is due to the Cn$^-$ ligand. In Cn$^\bullet$ it is absent and during oxidation of **1** the

band gradually disappears (Figure 7 (b)). ^{Py}Cn$^\bullet$ exhibits a broader band at 500-550 nm and a weaker

NIR band at 800 nm. Both bands are assigned to $\pi_{Ar} \to \pi_{NB}$ (singly occupied) charge transfer transitions

(Ar = aromatic and NB = non bonding). The changes of spectral features during ^{Py}Cn$^\bullet \to$ ^{Py}Cn$^+$ and

^{Py}Cn$^\bullet \to$ ^{Py}Cn$^-$ conversions were recorded by spectroelectrochemical measurements and are illustrated in

Figures 7(c) and 7(d). During both conversions the absorption band of ^{Py}Cn$^\bullet$ at 500-540 nm diminishes

significantly. In $^{Py}Cn^-$ the NIR band at 800 nm is absent, while in $^{Py}Cn^+$ it is hypsochromically shifted to 725 nm.

Catalytic Activity. $^{Py}Cn^\bullet$ has been established as a catalyst for the oxidative cleavage of benzil to benzoic acid in methanol in air. Oxidative cleavage of benzil to benzoic acid is not common, generally in presence of base benzil undergoes rearrangement to benzilic acid.[14] However the reaction of benzil (2.0 mmol) with $^{Py}Cn^\bullet$ (0.07 mmol) in methanol in presence of triethylamine (0.03 mmol) and air at RT for 48 h affords benzoic acid (3.44 mmol), corresponding to 86 % conversion (see, experimental section in SI). The plausible path of the catalysis is depicted in Chart 3. Reaction of benzil with $^{Py}Cn^\bullet$ produces $^{Py}Cn^+$ and a paramagnetic intermediate **G** that reacts with O_2 molecules and generates intermediate **H**.

Chart 3. Catalytic Cycle of the Oxidative Cleavage of Benzil to Benzoic Acid in Presence of $^{Py}Cn^\bullet$ and Et₃N in MeOH
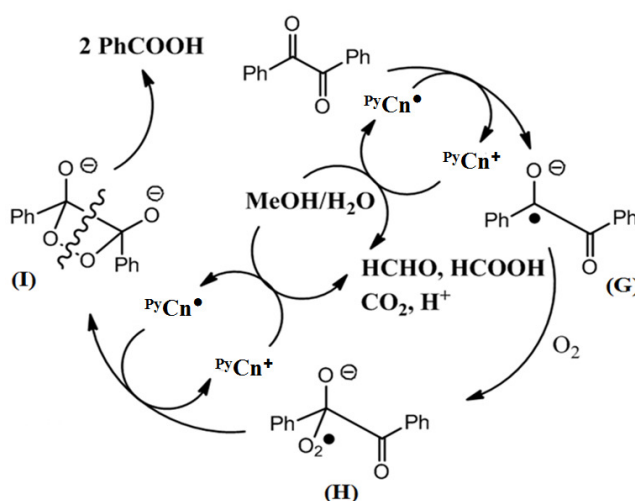
Reduction of **H** by another molecule of $^{Py}Cn^\bullet$ generates a dioxetane intermediate **I**. **I** is not stable and undergoes homolytic cleavage affording benzoic acid.[19] Existence of intermediates (**H**) and (**I**) was authenticated by ESI mass spectrometry of the crude reaction mixture after 48 h (see, Figure S9), where no mass peak due to the unreacted benzil was detected. Formation of benzoic acid was confirmed by single crystal X-ray crystallography.[20] $^{Py}Cn^+$ is an oxidizing agent ($E_{Cn+/Cn\bullet}$ = -0.34 V vs Fc$^+$/Fc couple) and the conversion of $^{Py}Cn^+$ to $^{Py}Cn^\bullet$ is achieved in MeOH which acts as a reducing agent (MeOH + H_2O = CO_2 + 6H$^+$ + 6e, E^0 = 0.02 V *vs* SHE).[21] The reaction of methanol with $^{Py}Cn^+$ generated from a

constant potential coulometric experiment was investigated by UV-Vis absorption spectra. It is observed that $^{Py}Cn^+$ reacts with methanol and the change of the absorption spectra of the mixture occurs with several isosbestic points as depicted in Figure S10.

Notably, the similar reaction of 2 2'-pyridil (0.5 m mol) with $^{Py}Cn^\bullet$ (0.03 m mol) in methanol in presence of triethylamine (0.02 mmol) and air at RT for 30 h affords picolinic acid in quantitative yields (Figure S11). Thus, $^{Py}Cn^\bullet$ has been established as a catalyst for the oxidative cleavage of 1,2-diketones to the corresponding acids.

Conclusion

A cascade route in isolating a new family of hetero-arene radicals as 1,2- benzodiazinyl radicals (cinnolinyl radicals) is disclosed. Two structurally different cinnolinyl radicals, $Cn^\bullet$ and $^{Py}Cn^\bullet$ were successfully isolated using 1,4-naphthoquinone as a precursor. Reaction of 1,4-naphthoquinoe with hydrazine hydrate is $(5e + 5H^+)$ redox cascade and affords $Cn^\bullet$, while the same with 2-hydrazino pyridine is a $(7e + 7H^+)$ oxidative cascade and affords $^{Py}Cn^\bullet$. The redox properties of $Cn^\bullet$ and $^{Py}Cn^\bullet$ are significantly different. $Cn^\bullet$ exhibits only cathodic wave due to $Cn^\bullet/Cn^-$ and $Cn^-/Cn^{\bullet 2-}$ redox couple, while $^{Py}Cn^\bullet$ in addition to the cathodic wave displays a reversible anodic wave due to $^{Py}Cn^+/^{Py}Cn^\bullet$ redox couple. Thus $^{Py}Cn^\bullet$ is a reducing agent and different from hydrazyl radicals. Similar to phenalenyl radical, $^{Py}Cn^\bullet$ exhibits three redox states, $^{Py}Cn^+$, $^{Py}Cn^\bullet$ and $^{Py}Cn^-$. $^{Py}Cn^\bullet$ is a catalyst promoting oxidative cleavage of benzil to benzoic acid in air. A Cn^- complex of copper(I) containing PPh$_3$ as coligands was successfully isolated, opening up an opportunity to compare the bond parameters and spectral features of $Cn^\bullet$ and Cn^-. $Cn^\bullet$ and $^{Py}Cn^\bullet$ are first paramagnetic neutral even alternate hetero-arenes and more stable than the phenalenyl radical that has been considered as a functional material in devising electronic devices and catalysts for several organic conversions. Thus isolation of $Cn^\bullet$ and $^{Py}Cn^\bullet$ is a breakthrough in organic radical chemistry.

Experimental Section

General Experimental Details

Reagents or analytical grade materials were obtained from the commercial suppliers and used without further purification. Spectroscopic grade solvents were used for spectroscopic and electrochemical measurements. The C, H and N contents of the compounds were obtained from a Perkin-Elmer 2400 Series II elemental analyzer. Infrared spectra of the samples were measured from 4000 to 400 cm^{-1} with KBr pellets at room temperature on a Perkin-Elmer Spectrum RX 1 FT-IR spectrophotometer. ^{1}H and ^{13}C NMR spectra in CDCl$_3$ solvent were recorded at 296 K on a Bruker Avance 500 MHz spectrometer. ESI mass spectra were recorded on a Shimadzu LCMS 2020 mass spectrometer equipped with electrospray ionization (ESI) ion source. Electronic absorption spectra in solution were obtained on a Perkin-Elmer Lambda 750 spectrophotometer in the range 3300-175 nm. The X-band EPR spectra were measured on a Magnettech GmbH MiniScope MS400 spectrometer (equipped with temperature controller TC H03), where the microwave frequency was measured with an FC400 frequency counter. The EPR spectra were simulated using Easy Spin software. The electro analytical instrument, BASi Epsilon-EC for cyclic voltammetric experiments in CH$_3$CN solutions containing 0.2 M tetrabutylammonium hexafluorophosphate as supporting electrolyte was used. The BASi platinum working electrode, platinum auxiliary electrode, Ag/AgCl reference electrode were used for the measurements. The redox potential data are referenced *vs.* ferrocenium/ferrocene, Fc$^+$/Fc, couple. BASi SEC-C thin layer quartz glass spectroelectrochemical cell kit (light path length of 1 mm) with platinum gauze working electrode and SEC-C platinum counter electrode were used for spectro-electrochemistry measurements.

Single crystals of ^{Py}Cn$^\bullet$ and **1**.½CH$_3$OH were picked up with a nylon loop and were mounted on Bruker AXS D8 QUEST ECO diffractometer equipped with a Mo-target rotating-anode X-ray source and a graphite monochromator (Mo-Kα, λ = 0.71073 Å). Final cell constants were obtained from least-squares fits of all measured reflections. Intensity data were corrected for absorption using intensities of redundant reflections. The structures were readily solved by direct methods and subsequent difference

Fourier techniques. The crystallographic data were listed in Table S1. The Siemens SHELXS-97 software package was used for solution, and SHELXL-97 was used for the refinement.[22] All non-hydrogen atoms were refined anisotropically. Hydrogen atoms were placed at the calculated positions and refined as riding atoms with isotropic displacement parameters.

All the calculations on $^{Py}Cn^{\bullet}$ reported in this article were done with the Gaussian 09W[23] program package supported by Gauss View 4.1. The DFT[24] calculations were performed at the level of Becke three parameters hybrid functional with the non-local correlation functional of Lee-Yang-Parr (B3LYP).[25] Gas-phase geometry of $^{Py}Cn^{\bullet}$ with doublet spin state was optimized using Pulay's Direct Inversion[26] in the Iterative Subspace (DIIS), 'tight' convergent SCF procedure[27] ignoring symmetry and the optimized coordinates are given in Tables S2-S4. Valence double zeta with diffuse and polarization functions, 6-31+G* as basis set[28] was employed for all the atoms for all the calculations.

The DFT calculations on $Cn^{\bullet}$, CnH, **1** and **1**$^{+}$ were performed with the ORCA program package[29] and the optimized coordinates are given in Table S5-S8. The gas phase geometries of **1** and CnH were optimized with singlet spin state, while $Cn^{\bullet}$ in CH_2Cl_2 and **1**$^{+}$ in gas phase were optimized with doublet spin state by hybrid PBE0 DFT method.[30] In case of **1** the coordinates obtained from the single crystal X-ray diffraction study were used as preliminary structures. For all calculations, the all-electron valence double-zeta, def2-SVP[31] basis set with "new" polarization function developed by Karlsruhe group was used for N, P, O, C and H atoms. For Cu atom def2-TZVP,[32] a valence triple-zeta basis set with new polarization function was used. Resolution of Identity (RIJCOSX)[33] approximation with def2/J auxiliary basis set for Coulomb and HF exchange integral for HF and hybrid DFT methods were employed for self-consistent field (SCF) gradient calculations.[34] The geometry optimizations were carried out in redundant internal coordinates without imposing symmetry constraints. The SCF calculations were converged tightly (1×10^{-8} Eh in energy, 1×10^{-7} Eh in the density change and 1×10^{-7} in maximum element of the DIIS error vector).

Synthesis and Catalysis

Benzo[g]naphtho[1,2-c]cinnolinyl-7,12,14-trione (Cn$^\bullet$) To a solution of 1,4-naphthoquinone (0.78 g, 5 mmol) in MeOH, hydrazine hydrate, 40% (0.312 g, 2.5 mmol $NH_2NH_2.H_2O$) was added, and the resulting mixture was stirred for 2 h at room temperature in air. A black solid of Cn$^\bullet$ separated out, which was filtered and dried in air. The obtained black mass was purified on an alumina column; the product was eluted using n-hexane-CH_2Cl_2 (9:1) solvent mixture and the mass obtained after evaporating solvent was used for further analyses. Yield: 0.56 g (~ 69 % with respect to 1,4-naphthoquinone). Anal. Calcd (%) for $C_{20}H_9N_2O_3$: C, 73.84; H, 2.79; N, 8.61; Found: C, 73.52; H, 2.71; N, 8.48. Mass spectrum (ESI): m/z, 325 for [Cn$^\bullet$, Figure S1]. IR/cm^{-1} (KBr): ν = 1680 (s), 1655 (s), 1578 (m), 1495 (s), 1435 (m), 1320 (m), 1210 (m), 1070 (m), 970 (s), 775 (m), 720 (m).

6-(pyridin-2-yl)-6,7-dihydrobenzo[g]naphtho[2,3-c] (5,8,13,14 tetraone) cinnolinyl radical (^{Py}Cn$^\bullet$): To a solution of 1,4-naphthoquinone (1.58 g, 10 mmol) in MeOH, 2-hydrazinopyridine (0.55 g, 5 mmol) was added, and the resulting mixture was stirred for 24 h at RT in air. A purple solid of ^{Py}Cn$^\bullet$ separated out, which was filtered and dried in air. Single crystals for X-ray analysis were prepared by the slow diffusion of n-hexane to the CH_2Cl_2 solution of ^{Py}Cn$^\bullet$ in a glass tube at 298 K. The crystals were used for further analyses. Yield: 1.50 g (~ 71% with respect to 1,4-naphthoquinone). Anal. Calcd (%) for $C_{25}H_{12}N_3O_4$: C, 71.77; H, 2.89; N, 10.04; Found: C, 71.50; H, 2.81; N, 9.93. Mass spectrum (ESI): m/z, 420 for [^{Py}Cn$^\bullet$]$^+$. IR/cm^{-1} (KBr): ν = 1685 (s), 1592 (s), 1505 (s), 1465 (m) 1430 (s), 1250 (m), 1170 (s), 1035 (m), 990 (s), 760 (m), 710 (m).

[Cu(Cn$^\bullet$)(PPh$_3$)$_2$] (1.½CH$_3$OH): To a solution of Cn$^\bullet$ (81 mg, 0.25 mmol) in CH_3OH (40 mL) in a 100 mL round-bottom flask were added carefully [Cu(PPh$_3$)$_3$Cl] (220 mg, 0.25 mmol) followed by triethylamine (1 drop, 0.50 mmol) and hydrazine hydrate (1 drop, 0.3 mmol). The solution turned green and it was allowed to evaporate slowly in air. After 2-3 days, black crystals of **1** separated out, which were collected upon filtration and dried in air. Yield: 130 mg (57% with respect to Cn$^\bullet$). Anal. Calcd for $C_{56}H_{39}N_2O_3P_2Cu$: C, 73.64; H, 4.30; N, 3.07. Found: C, 73.38; H, 4.16; N, 2.98. Mass spectrum (ESI):

m/z 912 for [**1**]$^+$. IR/cm^{-1} (KBr): ν 2930 (m), 1676 (s, CO), 1638 (s), 1565 (S), 1510 (m), 1290 (m), 1235(s), 1090 (m), 815 (m), 725 (s), 685 (s), 522 (s).

Catalytic Activity of ^{Py}Cn$^\bullet$. Oxidative Cleavage of Benzil to Benzoic Acid. To a solution of benzil (420 mg, 2 mmol) in methanol (40 ml), ^{Py}Cn$^\bullet$ (30 mg, 0.07 mmol) was added and mixture was stirred for 10 min at 298 K. The clear solution was allowed to evaporate slowly in air and after 48 h the residue obtained after evaporation of the solvent was purified on a basic alumina column. The colorless eluent obtained using pure CH_2Cl_2 as a solvent was collected and allowed to evaporate slowly in air. White needles of benzoic acid grown from the solution were collected and used for further analysis. Yield 420 mg (86 % with respect to benzil).

Oxidative Cleavage of 2 2'-Pyridil to Picolinic Acid. The reaction of 2 2'-pyridil (0.5 m mol) with ^{Py}Cn$^\bullet$ (0.03 m mol) in methanol in presence of triethylamine (0.02 mmol) and air at RT for 30 h affords picolinic acid in quantitative yields. In the mass spectrometry of the reaction mixture, a strong m/z peak due to picolinic acid was detected and no m/z peak due to 2 2'-pyridil was observed.

ASSOCIATED CONTENT

Supporting Information

X-ray crystallographic data, ESI mass spectra, thermal ellipsoid plots, EPR spectra, frontier molecular orbitals, change of UV-vis absorption spectra of ^{Py}Cn$^+$ in MeOH and gas phase optimized coordinates with the computed total energies, CIF files. This material is available free of charge via the Internet at http://pubs.acs.org.

AUTHOR INFORMATION

Corresponding Author

*Email: ghosh@pghosh.in; Phone: +91-33-2428-7347; Fax: +91-33-2477-3597

Author Contributions

The manuscript was written through contributions of all authors. All authors have given approval to the

final version of the manuscript.

Funding Sources

Notes

The authors declare no competing financial interests.

ACKNOWLEDGMENT

REFERENCES

(1) (a) Haddon, R. C. Design of Organic Metals and Superconductors. Nature. 1975, 256, 394-396. (b) Pal, S. K.; Itkis, M. E.; Tham, F. S.; Reed, R. W.; Oakley, R. T.; Haddon, R. C. Resonating Valence-Bond Ground State in a Phenalenyl-Based Neutral Radical Conductor. *Science*. **2005**, *309*, 281-284.

(2) (a) Pal, S. K.; Itkis, M. E.; Tham, F. S.; Reed, R. W.; Oakley, R. T.; Donnadieu, B.; Haddon, R. C. Phenalenyl-Based Neutral Radical Molecular Conductors: Substituent Effects on Solid-State Structures and Properties. *J. Am. Chem. Soc.* **2007**, *129*, 7163-7174. (b) Mandal, S. K.; Samanta, S.; Itkis, M. E.; Jensen, D. W.; Reed, R. W.; Oakley, R. T.; Tham, F. S.; Donnadieu, B.; Haddon, R. C. Resonating Valence Bond Ground State in Oxygen-Functionalized Phenalenyl-Based Neutral Radical Molecular Conductors. *J. Am. Chem. Soc.* **2006**, *128*, 1982-1994. (c) Chi, X.; Itkis, M. E.; Patrick, B. O.; Barclay, T. M.; Reed, R. W.; Oakley, R. T.; Cordes, A. W.; Haddon, R. C. The First Phenalenyl-Based Neutral Radical Molecular Conductor. *J. Am. Chem. Soc.* **1999**, *121*, 10395-10402.

(3) (a) Ahmed, J.; Chakraborty, S.; Jose, A.; Sreejyothi, P.; Mandal, S. K. Integrating Organic Lewis Acid and Redox Catalysis: The Phenalenyl Cation in Dual Role. *J. Am. Chem. Soc.* **2018**, *140*, 8330–8339. (b) Mukherjee, A.; Sen, T. K.; Ghorai, P. K.; Mandal, S. K. The non-innocent phenalenyl unit: an electronic nest to modulate the catalytic activity in hydroamination reaction. *Sci. Rep.* **2013**, *3*, 1-11. (c) Chirik, P. J.; Wieghardt, K. Radical Ligands Confer Nobility on Base-Metal Catalysts. *Science.* **2010**, *327*, 794-795.

(4) (a) Raman, K. V.; Kamerbeek, A. M.; Mukherjee, A.; Atodiresei, N.; Sen, T. K.; Lazic´, P.; Caciuc, V.; Michel, R.; Stalke, D.; Mandal, S. K.; Blügel, S.; Münzenberg, M.; Moodera, J. S. Interface-Engineered Templates for Molecular Spin Memory Devices. *Nature.* **2013**, *493*, 509-512. (b) Miyamachi, T.; Gruber, M.; Davesne, V.; Bowen, M.; Boukari, S.; Joly, L.; Scheurer, F.; Rogez, G.; Yamada, T. K.; Ohresser, P.; Beaurepaire, E.; Wulfhekel, W. Robust Spin Crossover and Memristance Across a Single Molecule. *Nat. Commun*. **2012**, *3*, 1-6.

(5) (a) Savva, A. C.; Mirallai, S. I.; Zissimou, G. A.; Berezin, A. A.; Demetriades, M.; Kourtellaris, A.; Constantinides, C. P.; Nicolaides, C.; Trypiniotis, T.; Koutentis, P. A. Preparation of Blatter Radicals via Aza-Wittig Chemistry: The Reaction of *N*-Aryliminophosphoranes with 1-(Het)aroyl-2-aryldiazenes. *J. Org. Chem.* **2017**, *82*, 7564-7575. (b) Kaszyn´ski, P.; Constantinides, C. P.; Young, V. G. The Planar Blatter Radical: Structural Chemistry of 1,4-Dihydrobenzo[*e*][1,2,4]triazin-4-yls. *Angew. Chem. Int. Ed.* **2016**, *55*, 1-5. (c) Morgan, I. S.; Peuronen, A.; Hänninen, M. M.; Reed, R. W.; Clérac, R.; Tuononen, H. M. 1-Phenyl-3-(pyrid-2-yl)benzo[*e*][1,2,4]triazinyl: The First "Blatter Radical" for Coordination Chemistry. *Inorg. Chem.* **2014**, *53*, 33-35.

(6) (a) Gautam, N.; Chourasia, O. P. Synthesis, Antimicrobial and Insecticidal Activity of Some New Cinnoline Based Chalcones and Cinnoline Based Pyrazoline Derivatives. *Indian J. Chem.* **2010**, *49*, 830-835. (b) Lewgowd, W.; Stanczak, A. Cinnoline Derivatives with Biological Activity. *Arch. Pharm. Chem. Life Sci.* **2007**, *340*, 65–80. (c) Barraja, P.; Diana, P.; Lauria, A.; Passannanti, A.; Almerico, A. M.; Minnei, C.; Longu, S.; Congiu, D.; Musiu, C.; La Colla, P. Indolo[3,2-c]cinnolines with Antiproliferative, Antifungal, and Antibacterial Activity. *Bioorg. Med. Chem.* **1999**, *7*, 1591-1596.

(7) (a) Ferlin, M. G.; Marzano, C.; Dalla Via, L.; Chilin, A.; Zagotto, G.; Guiotto, A.; Moro, S. New Water Soluble Pyrroloquinoline Derivatives as New Potential Anticancer Agents. *Bioorg. Med. Chem.* **2005**, *13*, 4733-4739. (b) Michael, J. P. Quinoline, Quinazoline and Acridone Alkaloids. *Nat. Prod. Rep.* **2005**, *22*, 627-646.

(8) Mathew, T.; Papp, A. A.; Paknia, F.; Fustero, S.; Surya Prakash, G. K. Benzodiazines: Recent Synthetic Advances. *Chem. Soc. Rev.* **2017**, *46*, 3060-3094.

(9) (a) Bai, J.; Yan, D.; Zhang, T.; Guo, Y.; Liu, Y.; Zou, Y.; Tang, M.; Liu, B.; Wu, Q.; Yu, S.; Tang, Y.; Hu, Y. *Angew. Chem. Int. Ed.* **2017**, *56*, 1-6. (b) Mondal, S.; Bera,S.; Maity, S.; Ghosh, P. Cobalt Ion Promoted Redox Cascade: A Route to Spiro Oxazine-Oxazepine Derivatives and a Dinuclear

Cobalt(III) Complex of an N-(1,4-Naphthoquinone)-*o*-aminophenol Derivative. *Inorg. Chem.* 2017, 56, 13194–13204.

(10) (a) Li, S-S.; Lv, X.; Ren, D.; Shao, C.-L.; Liuc, Q.; Xiao. J. Redox-Triggered Cascade Dearomative Cyclizations Enabled by Hexafluoroisopropanol. *Chem. Sci.* **2018**, DOI:10.1039/C8SC03339K. (b) Haibach, M. C.; Deb, I.; De, C. K.; Seidel. D. Redox-Neutral Indole Annulation Cascades. *J. Am. Chem. Soc*. **2011**, *133*, 2100-2103.

(11) Mondal, S.; Maity, S.; Ghosh, P. A Redox-Active Cascade Precursor: Isolation of a Zwitterionic Triphenylphosphonio-Hydrazyl Radical and an Indazolo-Indazole Derivative. *Inorg. Chem.* **2017**, 56, 8878–8888.

(12) (a) Hand, E. S; Cohen, T. Structural Elucidation of the Pentacyclic Cinnoline Obtained by the Reaction of 1,4-naphthoquinone with Hydrazine. *Tetrahedron* **1967**, *23*. 2911-2926. (b) Pummerer, R.; Pfaff, A.; Riegelbauer, G.; Rosenhauer, E. *Ber. Dtsch. Chem. Ges.* **1939**, *72*, 1623.

(13) (a) Hicks, R. G. Stable Radicals: Fundamentals and Applied Aspects of Odd-Electron Compounds; John Wiley & Sons: Wiltshire, U.K., **2010**. (b) Zilic, D.; Pajic, D.; Juric, M.; Molcanov, K.; Rakvin, B.; Planinic, P.; Zadro, K. Single Crystals of DPPH Grown from Diethyl Ether and Carbon Disulfide Solutions-Crystal Structures, IR, EPR and Magnetization Studies. *J. Magn. Reson*. **2010**, *207*, 34.

(14) Comisar, C. M.; Savage, P. E. The Benzil-Benzilic Acid Rearrangement in High-Temperature Water. *Green Chem*. **2005**, *7*, 800–806.

(15) (a) Tsuchiya, M.; Nomiyama, Y.; Takayoshi, W.; Iwami, Y.; Kanekiyo, Y. Colorimetric Sensing Method for Polyamines Utilising an Inclusion Complex of Stimuli-Responsive Amylose. *Anal. Methods*, **2011**, *3*, 524–528. (b) Goor, G., Glenneberg, J., Jacobi, S. Hydrogen Peroxide. *Ullmann's Encyclopedia of Industrial Chemistry*. **2007**, *18,* 393-427 (doi:10.1002/14356007.a13_443.pub2).

(16) (a) Shivakumar, M.; Pramanik, K.; Ghosh, P.; Chakravorty, A. Synthesis and Characterisation of a Pair of Azo Anion Radicals Bonded to Ruthenium(II). *Chem. Commun.*, **1998**, *19*, 2103-2104. (b) Shivakumar, M.; Pramanik, K.; Ghosh, P.; Chakravorty, A. Isolation and Structure of the First Azo Anion Radical Complexes of Ruthenium. *Inorg. Chem*, **1998**, *37*, 5968-5969.

(17) Villarreal, W.; Colina-Vegas, L.; Visbal, G.; Corona, O.; Correa, R. S.; Ellena, J.; Cominetti, M. R.; Batista, A. A.; Navarro. M. Copper(I)-Phosphine Polypyridyl Complexes: Synthesis, Characterization, DNA/HSA Binding Study, and Antiproliferative Activity. *Inorg. Chem.* **2017**, *56*, 3781−3793.

(18) For examples: (a) Lecontea, N.; Mouteta, J.; Herasymchuk, K.; Clarke, R. M.; Philouzea, C.; Luneau, D.; Storr, T.; Thomas, F. Mn(IV) and Mn(V)-Radical Species Supported by the Redox Non-innocent Bis(2-amino-3,5-di-*tert*-butylphenyl)amine Pincer Ligand. *Chem. Commun.* **2017**, *53*, 2764-2767. (b) Wang, Y.; Rajca, S.; Rajca, A. PEGylated, Water-Soluble, Stable Aminyl Radical**.** *J. Org. Chem.* **2017**, *82*, 7512−7518. (c) Sarkar, P.; Tiwari, A.; Sarmah, A.; Bhandary, S.; Roy, R. K.; Mukherjee, C. An Elusive Vinyl Radical Isolated as an Appended Unit in a Five-Coordinate Co(III)–Bis(iminobenzosemiquinone) Complex Formed *via* Ligand-Centered C–S Bond Cleavage. *Chem. Commun*. **2016**, *52*, 10613-10616. (d) Biswas, M. K.; Patra, S. C.; Maity, A. N.; Ke, S-C.; Das Adhikary, N.; Ghosh, P. Electronic Structures of Ruthenium and Osmium Complexes of 9,10-Phenanthrenequinone *Inorg. Chem*. **2012**, *51*, 6687-6699 and references therein. (e) Manner, V. W.; Markle, T. F.; Freudenthal, J. H.; Roth, J. P.; Mayer, J. M. The First Crystal Structure of a Monomeric Phenoxyl Radical: 2,4,6-tri-*tert*-butylphenoxyl Radical. *Chem. Commun.*, **2008**, 256-258. (f) Sokolowski, A.; Bothe, E.; Bill, E.; Weyhermüller, T.; Wieghardt, K. Phenoxyl Radical Complexes of Chromium(III). *Chem. Commun.* **1996**, 1671-1672.

(19) Liang, Y-F.; Jiao, N. Oxygenation via C-H/C-C Bond Activation with Molecular Oxygen. *Acc. Chem. Res.* **2017**, *50*, 1640−1653.

(20) a = 5.5122(18), b = 5.1369(15), c = 21.969(7), β = 97.065(9), V = 617.3(3), same as reported in Feld, R.; Lehmann, M. S.; Muir, K. W.; Speakman, J. C. The Crystal Structure of Benzoic Acid: a Redetermination with X-rays at Room Temperature; a Summary of Neutron-Diffraction Work at Temperatures Down to 5 K. *Zeitschrift für Kristallographie.* **1981**, *157*, 215-231.

(21) Iwasita, T. Electrocatalysis of Methanol Oxidation *Electrochimica Acta.* **2002**, *47*, 3663-3674.

(22) (a) Sheldrick, G. M. XS. Version 2013/1, Georg-August-Universität Göttingen, Göttingen, Germany, 2013. (b) Sheldrick, G. M. Acta crystallographica. Section A, Foundations and advances, **2015**, *71*, 3. (c) Sheldrick, G. M. *Acta Crystallographica Section C Structural Chemistry*, **2015**, *71*, 3.

(23)   Frisch, M. J.; Trucks, G. W.; Schlegel, H. B.; Scuseria, G. E.; Robb, M. A.; Cheeseman, J. R.; Montgomery, Jr., J. A.; Vreven, T.; Kudin, K. N.; Burant, J. C.; Millam, J. M.; Iyengar, S. S.; Tomasi, J.; Barone, V.; Mennucci, B.; Cossi, M.; Scalmani, G.; Rega, N.; Petersson, G. A.; Nakatsuji, H.; Hada, M.; Ehara, M.; Toyota, K.; Fukuda, R.; Hasegawa, J.; Ishida, M.; Nakajima, T.; Honda, Y.; Kitao, O.; Nakai, H.; Klene, M.; Li, X.; Knox, J. E.; Hratchian, H. P.; Cross, J. B.; Bakken, V.; Adamo, C.; Jaramillo, J.; Gomperts, R.; Stratmann, R. E.; Yazyev, O.; Austin, A. J.; Cammi, R.; Pomelli, C.; Ochterski, J. W.; Ayala, P. Y.; Morokuma, K.; Voth, G. A.; Salvador, P.; Dannenberg, J. J.; Zakrzewski, V. G.; Dapprich, S.; Daniels, A. D.; Strain, M. C.; Farkas, O.; Malick, D. K.; Rabuck, A. D.; Raghavachari, K.; Foresman, J. B.; Ortiz, J. V.; Cui, Q.; Baboul, A. G.; Clifford, S.; Cioslowski, J.; Stefanov, B. B.; Liu, G.; Liashenko, A.; Piskorz, P.; Komaromi, I.; Martin, R. L.; Fox, D. J.; Keith, T.; Al-Laham, M. A.; Peng, C. Y.; Nanayakkara, A.; Challacombe, M.; Gill, P. M. W.; Johnson, B.; Chen, W.; Wong, M. W.; Gonzalez, C.; Pople, J. A. *Gaussian 03, revision E.01*; Gaussian, Inc.: Wallingford, CT, 2004.

(24) (a) Parr, R. G.; Yang, W. Density Functional Theory of Atoms and Molecules; *Oxford University Press: Oxford, U.K.,* **1989**. (b) Salahub, D. R.; Zerner, M. C. The Challenge of d and f Electrons; *American Chemical Society: Washington, DC*, **1989**; *ACS Symposium Series 394*. (c) Kohn, W.; Sham, L. Self-Consistent Equations Including Exchange and Correlation Effects. *Phys. Rev.* **1965**, *140*,

A1133−A1138. (d) Hohenberg, P.; Kohn, W. Inhomogeneous Electron Gas. *Phys. Rev.* **1964**, *136*, B864−B871.

(25) (a) Becke, A. D. Density-Functional Thermochemistry. III. The Role of Exact Exchange. *J. Chem. Phys.* **1993**, *98*, 5648−5652. (b) Miehlich, B.; Savin, A.; Stoll, H.; Preuss, H. Results Obtained with the Correlation Energy Density Functionals of Becke and Lee, Yang and Parr. *Chem. Phys. Lett.* **1989**, *157*, 200−206. (c) Lee, C.; Yang, W.; Parr, R. G. Development of the Colle-Salvetti Correlation-Energy Formula into a Functional of the Electron Density. *Phys. Rev. B: Condens. Matter Mater. Phys.* **1988**, *37,* 785−789.

(26) Pulay, P. Improved SCF Convergence Acceleration. *J. Comput.Chem.* **1982**, *3,* 556−560.

(27) Schlegel, H. B.; McDouall, J. J. In Computational Advances in Organic Chemistry; Ogretir, C., Csizmadia, I. G., Eds.; *Kluwer Academic: Dordrecht, The Netherlands,* **1991**; 167−185.

(28) (a) Rassolov, V. A.; Ratner, M. A.; Pople, J. A.; Redfern, P. C.; Curtiss, L. A. 6-31G* Basis Set for Third-row Atoms. *J. Comput. Chem.* **2001**, *22*, 976−984. (b) Francl, M. M.; Pietro, W. J.; Hehre, W. J.; Binkley, J. S.; DeFrees, D. J.; Pople, J. A.; Gordon, M. S. Self-Consistent Molecular Orbital Methods. 23. A Polarization Basis Set for Second Row Elements. *J. Chem. Phys*. **1982**, *77,* 3654−3665. (c) Hariharan, P. C.; Pople, J. A. Accuracy of AHn Equilibrium Geometries by Single Determinant Molecular Orbital Theory. *Mol. Phys.* **1974**, *27*, 209−214. (d) Hariharan, P. C.; Pople, J. A. The Influence of Polarization Functions on Molecular Orbital Hydrogenation Energies. *Theor. Chim. Acta*. **1973**, *28*, 213−222.

(29) Neese, F. The ORCA Program System. *Wiley Interdiscip. Rev.: Comput. Mol. Sci.* **2012**, *2*, 73-78.

(30) (a) Becke, A. D. Density-Functional Thermochemistry. III. The Role of Exact Exchange. *J. Chem. Phys.* **1993**, *98*, 5648-5652. (b) Miehlich, B.; Savin, A.; Stoll, H.; Preuss, H. Results Obtained

with the Correlation Energy Density Functionals of Becke and Lee, Yang and Parr. *Chem. Phys. Lett.* **1989**, *157*, 200-206. (c) Lee, C.; Yang, W.; Parr, R. G. Development of the Colle-Salvetti Correlation-Energy Formula into a Functional of the Electron Density. *Phys. Rev. B* **1988**, *37*, 785-789.

(31) (a) Parr, R. G.; Yang, W. Density Functional Theory of Atoms and Molecules. Oxford University Press, Oxford. Oxford University Press: Oxford, U.K., 1989. (b) Salahub, D. R.; Zerner, M. C. The challenge of d and f electrons. Theory and computation. American Chemical Society: Washington, DC, 1989. (c) Kohn, W.; Sham, L. Self-Consistent Equations Including Exchange and Correlation Effects. *Phys. Rev.* **1965**, *140*, A1133-1138. (d) Hohenberg, P.; Kohn, W. Inhomogeneous Electron Gas. *Phys. Rev.* **1964**, *136*, B864-871.

(32) (a) Weigend, F.; Ahlrichs, R. Balanced Basis Sets of Split Valence, Triple Zeta Valence and Quadruple Zeta Valence Quality for H to Rn: Design and Assessment of Accuracy. *Phys. Chem. Chem. Phys.* **2005**, *7*, 3297-3305. (b) Weigend, F.; Furche, F.; Ahlrichs, R. Gaussian basis sets of quadruple zeta valence quality for atoms H–Kr. *J. Chem. Phys.* **2003**, *119(24)*, 12753-12762. (c) Eichkorn, K.; Weigend, F.; Treutler, O.; Ahlrichs, R. Auxiliary Basis Sets for Main Row Atoms and Transition Metals and Their Use to Approximate Coulomb Potentials. *Theor. Chem. Acc.* **1997**, *97*, 119-124. (d) Schaefer, A.; Huber, C.; Ahlrichs, R. Fully Optimized Contracted Gaussian Basis Sets of Triple Zeta Valence Quality for atoms Li to Kr. *J. Chem. Phys.* **1994**, *100(8)*, 5829-5835. (e) Schaefer, A.; Horn, H.; Ahlrichs, R. Fully Optimized Contracted Gaussian Basis Sets for Atoms Li to Kr. *J. Chem. Phys.* **1992**, *97*, 2571-2577.

(33) Kossmann, S.; Neese, F. Efficient Structure Optimization with Second-Order Many-Body Perturbation Theory: The RIJCOSX-MP2 Method. *J. Chem. Theory Comput.* **2010**, *6*, 2325-2338.

(34) Schlegel, H. B.; McDouall, J. J.; Ogretir, C., Csizmadia, I. G., in *Computational Advances in Organic Chemistry*, Eds.; Kluwer Academic: The Netherlands, 1991.

1
2
3
4
5
6
7
8
9
10
11
12
13
14
15
16
17
18
19
20
21
22
23
24
25
26
27
28
29
30
31
32
33
34
35
36
37
38
39
40
41
42
43
44
45
46
47
48
49
50
51
52
53
54
55
56
57
58
59
60

"For Table of Contents Only"